ROYAL SOCIETY OF CHEMISTRY

COMMUNICATION

Check for updates

Ultrastable sandwich graphene oxide hollow fiber membranes with confined interlayer spacing†

Wufeng Wu, Jingyi Su, Miaomiao Jia, Weiming Zhong, Zhanjun Li [iD] and Wanbin Li [iD] *

Graphene oxide (GO) membranes are extremely suitable for ultrafast molecular separation. However, the expansion of the GO interlayer spacing in aqueous solution causes poor rejection of small solutes and the risk of membrane dissociation. We reported a concept of constructing three-dimensional sandwich hollow fibers for confining the interlayer spacing and restraining swelling of GO membranes. Through coating the porous polymer *via* simple immersion-precipitation phase inversion, GO membranes are sandwiched between the porous coats and hollow fiber substrates. The out-of-plane swelling and interlayer-spacing expansion are suppressed bilaterally by the coats and substrates. Benefiting from the confined interlayer spacing of 0.86 nm, the sandwich GO membranes exhibit large permeance and impressive rejections over 97% and 98% for mono and multivalent salts, which are much higher than those of conventional GO membranes, usually less than 40%. Moreover, the sandwich GO membranes display substantially improved water stability and can maintain the high performance even under ultrasonic treatment.

Membrane processes can efficiently and precisely separate two-/multi-component mixtures through an environmentally friendly and energy-saving route. Various materials, including polymers, zeolites, and metal–organic frameworks, have been employed for preparing high-performance membranes.[1–4] Graphene and its derivatives, especially graphene oxide (GO), show great potential in fabrication of membranes with ultrafast and precise separation efficiency, thanks to its ultrathin structures, abundant hydrophilic groups and appropriate transport channels.[5,6] Ultrathin graphene-based membranes, with single-/few-layered structures, have been demonstrated with impressive permeance and rejection/selectivity in molecular separation, based on the artificial pores and intrinsic defects in nanosheets.[7–11] Unfortunately, it is very difficult to obtain a single-/few-layered membrane with

a large area for industrial application, not to mention simultaneously ensuring the homogeneity of the pore/defect size and membrane thickness. The stacked graphene-based membranes, obtained by facile and scalable coating or pressure filtration, can also be employed for nanofiltration, organic solvent nanofiltration, pervaporation, and gas separation.[12–20] These membranes are commonly composed of GO nanosheets, because the abundant oxygen-containing groups endow membranes with unique affinities for different molecules and the interlayer spacings offer pathways for selective molecular transport. The mass transfer channels of GO membranes consist of inner pores/defects, inter-edge gaps, and interlayer spacings. The interlayer spacing pathways from the superposition of GO nanosheets play a critical role in permselectivity.[21] However, because of the capillary suction for the liquid and solution in the separation application, GO membranes often become swollen and their interlayer spacing continues to increase.[22–24] These features cause poor rejection of salts and small solutes, and even lead to the dissociation of GO membranes.[24] Therefore, adjusting the transport pathways and enhancing the stability of GO membranes are of great scientific and practical interest.

Various methods involving chemical modification and physical fixation have been developed for controlling the interlayer spacing and improving the stability of GO membranes. Cross-linking modification and thermal reduction can restrict the interlayer spacing and enhance stability,[25–28] but the molecular separation capability for small molecules is still inferior compared with polymeric membranes. Morelos-Gomez *et al.* reported that polyvinyl alcohol could strengthen the adhesion between the GO layers and substrates through covalent or hydrogen bonding, and deoxycholate could enhance rejection by changing the membrane electrostatic potential.[29] Chen *et al.* demonstrated that the cation–π interaction could improve the water stability and fix the interlayer spacing of GO membranes.[30] In the static diffusion experiment, the GO membranes fixed by a smaller cation exhibited sharp sieving properties for other cations with larger hydrated volumes, yet there was no further study about the performance of the cation-

School of Environment, Guangdong Key Laboratory of Environmental Pollution and Health, Jinan University, Guangzhou 511443, P. R. China. E-mail: gandeylin@126.com

This journal is © The Royal Society of Chemistry 2019

J. Mater. Chem. A, 2019, 7, 13007–13011 | 13007

fixed GO membranes in pressure-driven filtration that has greater significance for practical application.

Physical fixation has reliable availability for regulating the permeation properties of GO membranes as well. The electric field can control water transport in the interlayer spacing, because the water molecules are ionized under current.[31] Applied pressure is an important parameter for the mass transfer property of GO membranes. A larger feed pressure commonly induces narrower interlayer spacing and higher salt rejection.[32] Abraham *et al.* encapsulated moist-exposed 100 μm-thick GO laminates with various interlayer spacings using epoxy.[33] The membranes showed accurate ion sieving properties in the static diffusion experiment, yet the architecture with vertically aligned GO laminates increased the cost and decreased the processability. Recently, by utilizing the anisotropic feature of GO membranes with out-of-plane unidirectional swelling, we reported an external pressure regulation strategy for suppressing swelling and interlayer-spacing expansion.[34] The GO flat membranes compressed by porous substrates displayed outstanding desalination performance for mono/multivalent salts in cross-flow filtration. But this strategy is inconvenient to implement in industrial spiral-wound and hollow fiber membrane modules. We envisage that a three-dimensional sandwich hollow fiber membrane with two exterior porous substrates and an intermediate GO layer will exhibit precise sieving properties for small solutes, because the two substrates can provide the opposite force to restrain the out-of-plane swelling and interlayer-spacing expansion. Moreover, since the GO layer is confined, the sandwich membrane is expected to have good stability.

The concept of three-dimensional construction of sandwich GO (SGO) hollow fiber membranes for controlling GO swelling and the interlayer-spacing variation is illustrated in Fig. 1a–c. The SGO hollow fiber membrane was fabricated in two steps: GO deposition by vacuum filtration and formation of the outer porous coat by immersion-precipitation phase inversion (Fig. S1, ESI†).[14,35] Polyvinylidene fluoride (PVDF) hollow fibers were first employed for supporting the GO membrane. After GO deposition and drying for 12 h, the GO/PVDF hollow fiber membrane was immersed in polysulfone (PSF) *N,N*-dimethylformamide (DMF) ink and then immersed into a water coagulant bath for phase-inversion. The formed PSF coat showed an asymmetric structure with an outer dense layer (Fig. S2, ESI†). During the exchange between DMF and water, the solvent migrating to the coagulant bath caused the bulk flow containing PSF chains. Therefore, the SGO/PVDF membrane prepared with a dried GO hollow fiber, named SGO-D/PVDF, had a loose three-tiered structure. The unrestricted gaps at the interface of different layers were harmful to control GO swelling. In order to prompt the PSF solidification to start at the GO side, the wetted GO/PVDF (GO-W/PVDF) membrane filled with water from vacuum filtration was applied for PSF phase-conversion coating. Because the water in the tube side served as a bore coagulant, the formed asymmetric PSF coat exhibited an inner dense layer (Fig. S2, ESI†). However, large interstices still existed between the PSF coat and GO layer. There might be two reasons for this phenomenon. First, the DMF solvent from the PSF solution led to the structural change of the PVDF hollow fiber. Second, the water diffusion from the tube side to polymeric solution was too slow to promote PSF coagulation completely; consequently the solidification in the water bath caused the out-migration of PSF chains. For reducing the possible structural change, the PVDF hollow fiber was ammoniated and cross-linked with ammonia (NPVDF) and then employed for preparation of the SGO membranes.[36] The NPVDF hollow fiber had excellent solvent resistance with small swelling of less than 2.0% in boiling DMF. The poor compatibility of the obtained SGO-W/NPVDF membrane indicated that the change
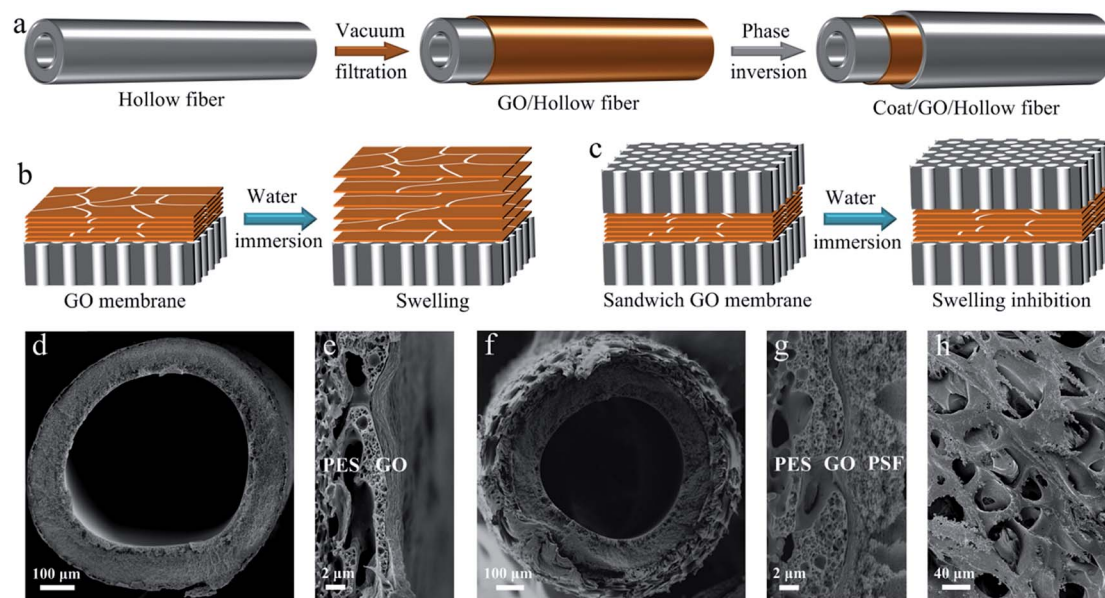
Fig. 1 SGO hollow fiber membranes. (a) The schematic of preparation of SGO hollow fiber membranes. (b and c) The schematics of GO membranes with increased interlayer spacing and SGO membranes with confined interlayer spacing in water. SEM images of (d and e) the GO/PES hollow fiber membrane and (f–h) the SGO-W/PES hollow fiber membrane.

13008 | *J. Mater. Chem. A*, 2019, **7**, 13007–13011

This journal is © The Royal Society of Chemistry 2019

in the fiber structure was not a dominant factor for the formation of large interstices (Fig. S3, ESI†). To accelerate the outward water diffusion, the polyether sulfone (PES) hollow fiber with larger permeability was applied as the substrate for preparing the SGO membranes (Fig. 1d and e). Expectedly, the GO and PSF layers of the SGO-D/PES membrane displayed inferior adhesion (Fig. S4, ESI†). While the prepared SGO-W/PES membrane showed a compact structure. SEM images present that the uniform PSF coat of the SGO-W/PES membrane had an inner dense/fingerlike structure and an outer macroporous surface (Fig. 1f–h). The GO layer was tightly clamped by the PSF coat and PES hollow fiber. It was noteworthy that the GO shrinkage from wet to dry states would bring about a gap theoretically, yet this speculation did not occur in experiment. In order to investigate the mechanism, we fabricated the PSF flat membrane by immersion-precipitation phase inversion and measured its dimensional variation during preparation. The result revealed that the dimensions of the PSF membrane shrunk by 10% after drying. This might be the reason for the compact SGO-W/PES membrane. The synchronous contraction of the PSF coat occupied the possible void region from GO shrinkage. After immersing the dried PSF membrane in water, the dimensions showed hardly any change, which would be beneficial to inhibit the GO swelling and interlayer-spacing variation.

The swelling properties of GO membranes were studied using an optical microscope (Fig. 2a). For better observation, a thicker GO membrane was deposited on the hollow fiber. After immersion in water for 1 h, the GO layer detached from the GO/PES hollow fiber and showed obvious swelling (Fig. S5, ESI†), which would result in drastic performance degradation of GO membranes. The thickness expanded to about five times the original one. In contrast, the SGO-W/PES membrane after water immersion for 1 h showed a constant structure. The thickness of the GO layer remained almost unchanged, revealing that the construction of sandwich membranes could substantially enhance the stability and inhibit the swelling of GO membranes in water. X-ray diffraction (XRD) was employed to investigate the interlayer spacing of the GO membranes (Fig. 2b). The dry GO/PES and SGO-W/PES membranes had a similar interlayer spacing of 0.80 nm. For the 1 h wetted GO/PES membrane, because the adsorbed water disordered the arrangement of GO

nanosheets, the membrane presented an amorphous structure. For the SGO-W/PES membrane, the water exposure did not obviously change the arrangement of GO nanosheets. The wetting only resulted in a slight extension of the interlayer spacing by 0.06 nm. Considering the intrinsic thickness (0.34 nm) of graphene nanosheets, the free spacing between two carbon planes of the wetted SGO-W/PES membranes was 0.52 nm, which was smaller than the hydrated diameters of various salt cations, such as 0.71 nm Na^+. The robust sandwich GO membranes with confined interlayer spacing and non-swelling properties are highly expectable with a strong probability for desalination.

The desalination performance of the prepared membranes was evaluated by dead-end filtration (Fig. 3). The SGO-W/PES hollow fiber membrane exhibited a much higher NaCl rejection of 95.0% than the GO/PES membrane at room temperature and 2.0 bar (Fig. 3a), despite the decline in water permeance from 14.6 to 7.1 L per m^2 per h per bar, implying the significance of PSF-coat restriction for membrane performance. The poor rejection of the PSF/PES hollow fiber, which was fabricated by a similar coating process but without GO deposition, proved that the superior rejection should be ascribed to the confined GO layer rather than the polymeric substrate and coat. The SGO-W/PES membrane displayed more precise ion sieving properties and a faster mass transfer process than the SGO-D/PES membrane, due to the narrower interlayer spacing of the GO layer and superior porous structure of the PSF coat. It should be noted that the salt rejection of the SGO-W/PES membrane was higher than that of most reported GO membranes in previous studies.[12,13,15,16,18,22] The epoxy-encapsulated GO laminates showed similar impressive rejection in the static diffusion experiment, but there was no further performance evaluation in pressure-driven filtration,[33] which usually brought about relatively poor rejection.[37] Although the pressure-regulated GO membranes exhibited high desalination performance,[34] the imposed high-resolution pressure might reduce the availability of this concept in industrial application. Besides the outstanding filtration performance, the sandwich GO hollow fiber membranes possessed the merits of good processibility, excellent operability and large area per volume as well. Because of the existence of interstices between PSF coats and GO layers, the sandwich membranes prepared with other substrates and processes had ordinary rejection and permeance (Fig. S6, ESI†). In addition to NaCl, some other salt solutions were used to evaluate the desalination performance of the SGO-W/PES membrane. The $MgCl_2$, $MgSO_4$ and Na_2SO_4 rejections reached as high as 94.7%, 95.2% and 97.0% at 2.0 bar, respectively (Fig. 3b). The slightly higher rejection of Na_2SO_4 over $MgSO_4$ and NaCl over $MgCl_2$ suggested that Donnan exclusion based on electrostatic repulsion played a role in separation more or less, besides the main size exclusion. With the increase of salt concentration, the rejection and permeance degenerated synchronously (Fig. 3c). This was explained by the increased osmotic pressure and concentration polarization. Unlike polymeric membranes and conventional GO membranes with higher rejection under a larger feed pressure,[32,38] the separation efficiency of the SGO-W/PES membrane decreased as the pressure increased (Fig. 3d). This phenomenon was attributed to the unique structure and non-
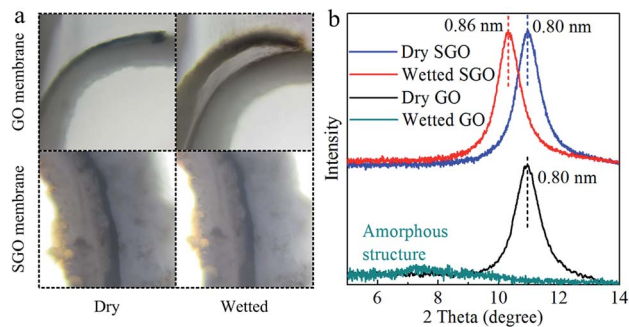
Fig. 2 Swelling properties and interlayer spacing. (a) Optical microscopy images of the dry and 1 h wetted GO/PES and SGO-W/PES hollow fiber membranes. (b) XRD patterns of the dry and 1 h wetted GO/PES and SGO-W/PES hollow fiber membranes.
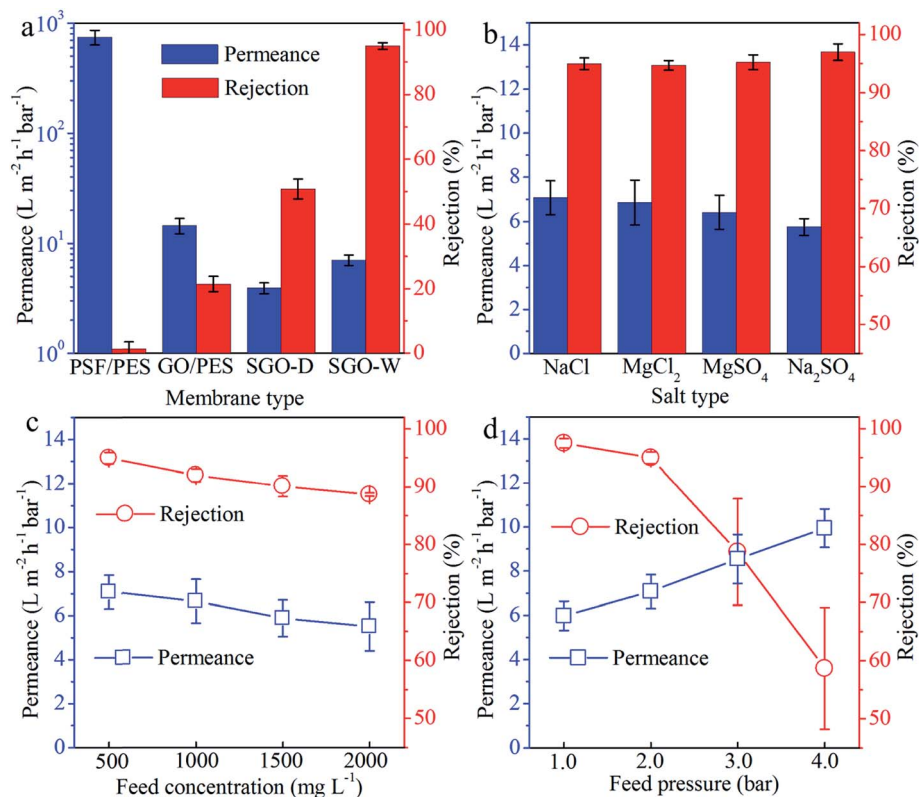
Fig. 3 Desalination performance. (a) Desalination performance of various membranes with a PES hollow fiber substrate. The PSF/PES hollow fiber was fabricated by a similar coating process to the SGO-W/PES membrane but without GO deposition. (b) Permeance and rejection of various salt solutions through the SGO-W/PES hollow fiber membrane with a feed pressure of 2.0 bar. (c) The effect of NaCl concentration on desalination performance of the SGO-W/PES hollow fiber membrane at 2.0 bar. (d) Water permeance and NaCl rejection of the SGO-W/PES membrane under different feed pressures.

swelling mechanism of sandwich GO membranes (Fig. S7, ESI†). For the sandwich membrane with a three layered structure, the GO layer with the greatest mass transfer resistance caused the largest pressure drop. When the feed pressure increased, the PES hollow fiber shrunk, yet the PSF coat remained almost constant, which could be verified by the existence of the gap between the PSF coat and GO layer of the sandwich membrane after filtration with high pressure (Fig. S7b, ESI†). The difference in shrinkage of different layers offered space for GO swelling, so the rejection decreased while permeance increased with increasing pressure. At 1.0 bar, the NaCl, MgCl$_2$, MgSO$_4$ and Na$_2$SO$_4$ rejections were up to 97.5%, 98.0%, 98.5% and 99.1%, respectively (Fig. S8, ESI†).

As mentioned above, the instability of GO membranes in water purification is a serious bottleneck for their application. For testing the stability of the sandwich membranes, the long-term separation performance was measured accompanied by an intermittent ultrasonic treatment (Fig. 4), which was generally employed for GO exfoliation. Instead of performance deterioration, the ultrasonic treatment improved rejection and permeance owing to the alleviated concentration polarization. The SGO-W/PES membrane maintained the high rejection and permeance over 3 days and five times of ultrasonic treatment. Even upon lengthening the filtration duration to 18 days, the membrane still displayed only small fluctuations in rejection and permeance (Fig. S9, ESI†). The impressive desalination performance and
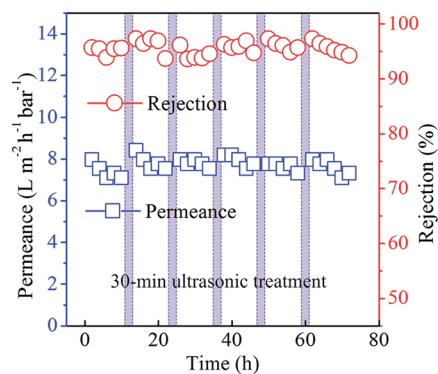
Fig. 4 Long-term stability of the SGO-W/PES membrane at 2.0 bar. The separation performance showed a small fluctuation over 3 days and ultrasonic treatment five times.

high water stability confirmed the feasibility of three-dimensional construction of sandwich GO hollow fiber membranes.

Conclusions

In summary, we have reported a concept of three-dimensional construction for controlling anisotropic structural change, based on fabrication of sandwich hollow fiber membranes for confining the interlayer spacing and restraining swelling of GO

membranes. The outer porous coats and inner hollow fibers not only suppress the structural variation of GO membranes in water, but also provide mass transfer channels for filtration. The prepared sandwich GO membranes exhibited admirable desalination performance for mono/multivalent salt solutions and robust water stability even under ultrasonic treatment. Our work offers an alternative route to control the GO swelling and interlayer spacing for separation applications.

Conflicts of interest

The authors declare no competing financial interests.

Acknowledgements

Notes and references

1 K. P. Lee, T. C. Arnot and D. Mattia, *J. Membr. Sci.*, 2011, **370**, 1–22.
2 K. L. Cho, A. J. Hill, F. Caruso and S. E. Kentish, *Adv. Mater.*, 2015, **27**, 2791–2796.
3 X. Liu, N. K. Demir, Z. Wu and K. Li, *J. Am. Chem. Soc.*, 2015, **137**, 6999–7002.
4 W. Li, *Prog. Mater. Sci.*, 2019, **100**, 21–63.
5 B. Mi, *Science*, 2014, **343**, 740–742.
6 G. Liu, W. Jin and N. Xu, *Chem. Soc. Rev.*, 2015, **44**, 5016–5030.
7 S. P. Surwade, S. N. Smirnov, I. V. Vlassiouk, R. R. Unocic, G. M. Veith, S. Dai and S. M. Mahurin, *Nat. Nanotechnol.*, 2015, **10**, 459–464.
8 L. Wang, C. M. Williams, M. S. H. Boutilier, P. R. Kidambi and R. Karnik, *Nano Lett.*, 2017, **17**, 3081–3088.
9 P. R. Kidambi, D. Jang, J. C. Idrobo, M. S. H. Boutilier, L. Wang, J. Kong and R. Karnik, *Adv. Mater.*, 2017, **29**, 1700277.
10 G. Wei, X. Quan, S. Chen and H. Yu, *ACS Nano*, 2017, **11**, 1920–1926.
11 S. C. O'Hern, D. Jang, S. Bose, J. C. Idrobo, Y. Song, T. Laoui, J. Kong and R. Karnik, *Nano Lett.*, 2015, **15**, 3254–3260.
12 H. Huang, Z. Song, N. Wei, L. Shi, Y. Mao, Y. Ying, L. Sun, Z. Xu and X. Peng, *Nat. Commun.*, 2013, **4**, 2979.
13 Y. Han, Z. Xu and C. Gao, *Adv. Funct. Mater.*, 2013, **23**, 3693–3700.
14 K. Huang, G. Liu, Y. Lou, Z. Dong, J. Shen and W. Jin, *Angew. Chem., Int. Ed.*, 2014, **53**, 6929–6932.
15 A. Akbari, P. Sheath, S. T. Martin, D. B. Shinde, M. Shaibani, P. C. Banerjee, R. Tkacz, D. Bhattacharyya and M. Majumder, *Nat. Commun.*, 2016, **7**, 10891.
16 K. Goh, W. Jiang, H. E. Karahan, S. Zhai, L. Wei, D. Yu, A. G. Fane, R. Wang and Y. Chen, *Adv. Funct. Mater.*, 2015, **25**, 7348–7359.
17 L. Huang, J. Chen, T. Gao, M. Zhang, Y. Li, L. Dai, L. Qu and G. Shi, *Adv. Mater.*, 2016, **28**, 8669–8674.
18 W. L. Xu, C. Fang, F. Zhou, Z. Song, Q. Liu, R. Qiao and M. Yu, *Nano Lett.*, 2017, **17**, 2928–2933.
19 F. Zhou, H. N. Tien, W. L. Xu, J. T. Chen, Q. Liu, E. Hicks, M. Fathizadeh, S. Li and M. Yu, *Nat. Commun.*, 2017, **8**, 2107.
20 Q. Yang, Y. Su, C. Chi, C. T. Cherian, K. Huang, V. G. Kravets, F. C. Wang, J. C. Zhang, A. Pratt, A. N. Grigorenko, F. Guinea, A. K. Geim and R. R. Nair, *Nat. Mater.*, 2017, **16**, 1198–1202.
21 N. Wei, X. Peng and Z. Xu, *ACS Appl. Mater. Interfaces*, 2014, **6**, 5877–5883.
22 R. K. Joshi, P. Carbone, F. C. Wang, V. G. Kravets, Y. Su, I. V. Grigorieva, H. A. Wu, A. K. Geim and R. R. Nair, *Science*, 2014, **343**, 752–754.
23 S. Zheng, Q. Tu, J. J. Urban, S. Li and B. Mi, *ACS Nano*, 2017, **11**, 6440–6450.
24 C. N. Yeh, K. Raidongia, J. Shao, Q. H. Yang and J. Huang, *Nat. Chem.*, 2015, **7**, 166–170.
25 W. S. Hung, C. H. Tsou, M. De Guzman, Q. F. An, Y. L. Liu, Y. M. Zhang, C. C. Hu, K. R. Lee and J. Y. Lai, *Chem. Mater.*, 2014, **26**, 2983–2990.
26 H. Liu, H. Wang and X. Zhang, *Adv. Mater.*, 2015, **27**, 249–254.
27 L. Huang, Y. Li, Q. Zhou, W. Yuan and G. Shi, *Adv. Mater.*, 2015, **27**, 3797–3802.
28 K. H. Thebo, X. Qian, Q. Zhang, L. Chen, H. M. Cheng and W. Ren, *Nat. Commun.*, 2018, **9**, 1486.
29 A. Morelos-Gomez, R. Cruz-Silva, H. Muramatsu, J. OrtizMedina, T. Araki, T. Fukuyo, S. Tejima, K. Takeuchi, T. Hayashi, M. Terrones and M. Endo, *Nat. Nanotechnol.*, 2017, **12**, 1083–1088.
30 L. Chen, G. Shi, J. Shen, B. Peng, B. Zhang, Y. Wang, F. Bian, J. Wang, D. Li, Z. Qian, G. Xu, G. Liu, J. Zeng, L. Zhang, Y. Yang, G. Zhou, M. Wu, W. Jin, J. Li and H. Fang, *Nature*, 2017, **550**, 380–383.
31 K. G. Zhou, K. S. Vasu, C. T. Cherian, M. Neek-Amal, J. C. Zhang, H. Ghorbanfekr-Kalashami, K. Huang, O. P. Marshall, V. G. Kravets, J. Abraham, Y. Su, A. N. Grigorenko, A. Pratt, A. K. Geim, F. M. Peeters, K. S. Novoselov and R. R. Nair, *Nature*, 2018, **559**, 236–240.
32 Y. Wei, Y. Zhang, X. Gao, Y. Yuan, B. Su and C. Gao, *Carbon*, 2016, **108**, 568–575.
33 J. Abraham, K. S. Vasu, C. D. Williams, K. Gopinadhan, Y. Su, C. T. Cherian, J. Dix, E. Prestat, S. J. Haigh, I. V. Grigorieva, P. Carbone, A. K. Geim and R. R. Nair, *Nat. Nanotechnol.*, 2017, **12**, 546–550.
34 W. Li, W. Wu and Z. Li, *ACS Nano*, 2018, **12**, 9309–9317.
35 Q. Z. Zheng, P. Wang, Y. N. Yang and D. J. Cui, *J. Membr. Sci.*, 2006, **286**, 7–11.
36 W. Li, P. Su, Z. Li, Z. Xu, F. Wang, H. Ou, J. Zhang, G. Zhang and E. Zeng, *Nat. Commun.*, 2017, **8**, 406.
37 W. Hirunpinyopas, E. Prestat, S. D. Worrall, S. J. Haigh, R. A. W. Dryfe and M. A. Bissett, *ACS Nano*, 2017, **11**, 11082–11090.
38 W. Jin, A. Toutianoush and B. Tieke, *Langmuir*, 2003, **19**, 2550–2553.